Bimodal Hydrographs in Semi-humid Forested Watershed: Characteristics and Occurrence Conditions

Zhen Cui[1], Fuqiang Tian[1*], Zilong Zhao[1], Zitong Xu[1], Yongjie Duan[1], Jie Wen[2], Mohd Yawar Ali Khan[3]

[1] Department of Hydraulic Engineering & State Key Laboratory of Hydroscience and Engineering, Tsinghua University, Beijing 100084, China.

[2] State Key Laboratory of Simulation and Regulation of Water Cycle in River Basin, China Institute of Water Resources and Hydropower Research, Beijing 100038, China.

[3] Department of Hydrogeology, Faculty of Earth Sciences, King Abdulaziz University, Jeddah 21589, Saudi Arabia.

Corresponding author: Fuqiang Tian (tianfq@tsinghua.edu.cn)

Key Points:

- The stormflow hydrograph of the studied watershed displays a bimodal pattern.
- The onset of the bimodal response demonstrates a threshold behavior.
- Delayed stormflow is mainly contributed by shallow groundwater.

Abstract

Bimodal runoff behavior, characterized by two distinct peaks in flow response, often leads to significant stormflow and associated flooding. Understanding and characterizing this phenomenon is crucial for effective flood forecasting. However, this runoff behavior has been understudied and poorly understood in semi-humid regions. In this study, we investigated the response characteristics and occurrence conditions of bimodal hydrograph based on the hydrometric and isotope data spanning 10 years in a semi-humid forested watershed in North China. The main findings include: 1) the onset of the bimodal hydrograph exhibits a threshold behavior, with delayed streamflow peaks occurring when the sum of event rainfall (P) and antecedent soil moisture index prior to the rainfall (ASI) exceeds 200 mm; 2) isotopic hydrograph separation reveals that delayed stormflow process is primarily driven by pre-event water, with increasing contributions of pre-event water during catchment wetting-up; 3) the dynamic variation in groundwater level precedes that of streamflow, establishing a hysteretic relationship wherein groundwater level peaks before streamflow during delayed stormflow. These findings, supported by onsite observations, emphasize the dominance of shallow groundwater flow in the generation of delayed stormflow.

Keywords: Semi-humid watershed, Stormflow, Bimodal runoff response, Threshold, Shallow groundwater

1. Introduction

Runoff generation is one of the most complex hydrological processes due to their complexity and non-linearity (McDonnell *et al.*, 2007; McGuire & McDonnell, 2010; Phillips, 2003). At

different times of a year, the activation of different runoff generating mechanisms, and contrasting compartments and flow routes form different hydrograph shapes, which are generally classified as unimodal and bimodal response types (Jenkins *et al.*, 1994; Gu, 1996; Kosugi *et al.*, 2011). A unimodal response is characterized by a needle-shaped peak which responds immediately to the rainfall impulse. In contrast, the bimodal response contains a delayed damped arch-shaped peak responding to the same rainfall impulse in addition to the direct peak (Martínez-Carreras *et al.*, 2016). Generally, the delayed peak in a bimodal event contributes substantially more runoff than the first peak (Zillgens *et al.*, 2007). For instance, the study by Onda *et al.* (2001) showed that the delayed peak discharge is five to ten times greater than the first peak. When the bimodal runoff event occurs, the streamflow increases markedly and lasts for several days. Therefore, characterizing the bimodal response is of great significance to understanding the runoff generation process and essential to achieving improved forecasting of extreme floods.

Since the bimodal hydrograph was accidently observed in Côte d'Ivoire in 1960 during flood frequency analysis and surface runoff generation study (Dubreuil, 1960, 1985), bimodal response has piqued the interest of many hydrologists worldwide and been recorded in watersheds with varied geological and climate conditions. For example, Onda *et al.* (2001) observed bimodal hydrographs in a steep mountainous watershed underlain by shale and serpentinite in Japan (annual precipitation: 1800 mm). Padilla *et al.* (2014, 2015) found delayed peaks after the rainfall in a steep headwater catchment underlain by fractured bedrock also in Japan (annual precipitation: 2669 mm). Zillgens *et al.* (2007) recorded a delayed peak after the direct peak in Saalach basin in the Austrian Alps (annual precipitation: 1400 mm). Masiyandima *et al.* (2003) found bimodal responses in an inland valley watershed with wet lowlands in central Côte d'Ivoire (annual rainfall: 1045 mm). Anderson and Burt (1977, 1978) observed delayed peak after the storm at Bicknoller

Combe in Sommerset, composed of impermeable Old Red Sandstone. The characteristics and conditions of occurrence of bimodal hydrograph can provide an effective method for simplifying the description of complex hydrological systems, and comparing stormflow generation mechanism in different watersheds (Tromp-van Meerveld & McDonnel, 2006). However, most of these studies mentioned above have been done in humid regions with rainfall of more than 1000 mm. To the best of authors' knowledge, very few studies if not none have been conducted in semi-humid environment with rainfall less than 800 mm.

Meanwhile, recognizing the pivotal role of bimodal response in runoff generation, researchers have made concerted efforts over the past several decades to quantify its characteristics and establish statistical metrics for identifying the occurrence of bimodal events. Findings suggest that indicators for bimodal response encompass factors such as rainfall amount (Haga *et al.*, 2005), pre-event streamflow (Graeff *et al.*, 2009), soil moisture (Anderson & Burt, 1978; Weyman, 1970), groundwater level (Padilla *et al.*, 2015) and storage (Martínez-Carreras *et al.*, 2016). Taking the work of Martínez-Carreras *et al.* (2016) as an illustrative example, it revealed that the delayed peak manifested only when the watershed storage reached a critical threshold of 113 mm. It is noteworthy that predictors vary significantly among watersheds, with only a limited number of studies presenting quantitative results akin to those reported by Martínez-Carreras *et al.* (2016). Moreover, response timing metrics such as response lag to peak—providing insights into different aspects of water travel time during an event—have received comparatively less attention in the evaluation of threshold effects (Dingman, 2015; Ross *et al.*, 2021).

Many studies have delved into the compartments and flow pathways responsible for generating distinct runoff response patterns. The first runoff peaks are attributed to factors such as rainwater directly falling onto the stream channel, rapid flow through preferential paths (Becker

& McDonnell, 1998; Martínez-Carreras *et al.*, 2015; Wrede *et al.*, 2015), or saturation-excess overland flow in the riparian zone (Anderson & Burt, 1978; Westhoff *et al.*, 2011). While delayed runoff peaks in bimodal events are primarily linked to subsurface flow processes (Weyman, 1970; Onda *et al.*, 2006; Zillgens *et al.*, 2007; Graeff *et al.*, 2009; Padilla *et al.*, 2015). However, a notable gap exists in the literature, as many studies have focused solely on water flow processes within the soil profile without thoroughly investigating whether subsurface stormflow originates from the soil layer, bedrock layer, or a combination of both.

Bimodal responses, representing the nonlinear interplay between runoff and rainfall, inherently showcase the stormflow process in terms of both response timing and magnitude. This intuitive manifestation holds significant implications for advancing runoff modeling (Graeff *et al.*, 2009; McDonnell *et al.*, 2007) and enhancing the precision of flash flood forecasting (Zhang *et al.*, 2021; Zillgens *et al.*, 2007). In our present study, spanning the years 2014 to 2023, we collected data on rainfall, groundwater levels, soil water content, and streamflow within a semi-humid forest experimental watershed in North China. Our investigation involves characterizing the response magnitude and timing of stormflow to rainfall through hydrograph analysis, while also scrutinizing the composition of the water sources contributing to stormflow. Specifically, we hypothesize that (1) the occurrence of bimodal streamflow responses exhibits a threshold behavior with rainfall and watershed wetness, and (2) the primary source of water for the delayed stormflow is subsurface flow.

2. Materials and Methods

2.1 Study area

The study headwater catchment, the Xitaizi Experimental Watershed (XEW), is situated at coordinates 40°32′N and 116°37′E, as depicted in Figure 1. Spanning an area of 4.22 km^2, XEW exhibits elevations ranging from 676 to 1201 m above sea level. Approximately 54% of the area features a slope between 20% and 40%. The region experiences a monsoon-influenced semi-humid climate characterized by an average annual rainfall of 625 mm. The majority of this precipitation, around 80%, occurs between June and September. The annual mean temperature in the area is 11.5°C, accompanied by a relative humidity of 59.1%. Experimental and observational activities were conducted over the period from 2014 to 2023.

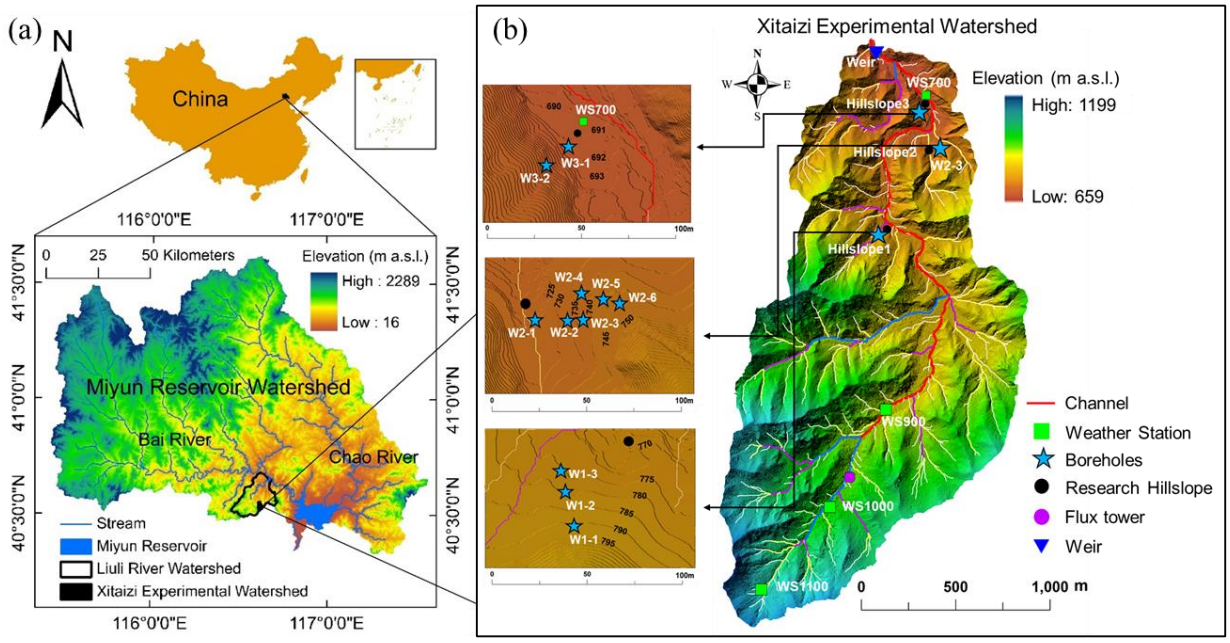

Figure 1. Location of the Xitaizi Experimental Watershed (XEW) in North China (a), and the detailed distributed monitoring stations and instruments (b), including four automatic weather stations (WS700-1100), one weir, and eleven groundwater boreholes (blue star corresponds with well numbers and locations). Four rain gauges are located near the weather stations, and one is located adjacent to the weir.

XEW represents a typical location in North China's earth-rocky mountainous region, where approximately 80% of the catchment area is underlain by firmly compacted, deeply weathered granite. Soil mapping and field investigations reveal the prevalent soil types to be brown earth and cinnamon soil (according to Chinese soil taxonomy), with a depth extending to 1.5 meters. The saturated hydraulic conductivity of the soil ranges from 19.5 to 175.3 mm/h, with an average value of 45 mm/h. The bedrock in the area is primarily composed of granite, constituting approximately 88% of the total bedrock composition, while gneiss and dolomite are sporadically distributed. Some sections of the granite exhibit fracture, and a layer of regolith is sandwiched between the soil layer and the bedrock layer. In terms of land cover, the catchment is predominantly covered by forest (98%), with 54.2% being broad-leaved, 2.3% coniferous, and 10.5% a mix of coniferous and broad-leaved. The remaining 33% consists of shrubs (Tie *et al.*, 2017).

2.2 Meteorology and runoff measurements

Meteorological variables and runoff have been systematically monitored since 2013. Meteorological conditions were consistently measured using four GRWS100 automatic weather stations. These weather stations were strategically distributed quasi-uniformly along the elevation gradient, as depicted in Figure 1. The comprehensive data collection from these stations contributes to a thorough understanding of the meteorological dynamics in the study area over the specified timeframe.

For the measurement of air temperature (*Ta*) and relative humidity at each automatic weather station, an HC2S3-L temperature and relative humidity probe was utilized. These probes were equipped with a radiation shield to enhance accuracy. Simultaneously, a LI-190R quantum sensor was employed to measure photosynthetically active radiation (PAR). Rainfall data were collected at 10-minute intervals using six tipping-bucket rain gauges. These gauges were positioned in an

144 open space near the automatic weather stations, and average values were adopted for analysis in
145 this study.

146 Furthermore, the antecedent precipitation index (API), generally used to represent the residual
147 effect of previous precipitation (Mosley, 1979; Iwagami *et al.*, 2010), was calculated for all the
148 events over 3, 6, and 12 days. The API during the antecedent *t* days is described as follows:

149 $$\mathrm{API}\ (t) = \sum_{i=1}^{t} \frac{P_i}{i} \quad (1)$$

150 where i is the day count and P_i is the daily precipitation in the i^{th} day previously.

151 A Parshall flume was installed at the catchment outlet to measure streamflow (Figure 1). The
152 water level in the flume was measured every 5 min with a HOBO capacitance water level logger
153 from 2014. Streamflow was calculated using the standard Parshall flume rating curve, and both
154 the rainfall and streamflow measurements were averaged to hourly timesteps, and in this study,
155 the analysis is conducted at hourly timesteps. Unfortunately, the observation equipment is
156 susceptible to failures due to the complex environmental conditions and disturbances caused by
157 wild animals and plants. Compounded by the remote location of XEW, accessing the site promptly
158 to address malfunctions is challenging, leading to the loss of some observation data. Notably,
159 stormflow data from July 19 to August 16, 2016, had to be excluded because the road collapsed
160 during a heavy storm, preventing a significant amount of runoff from passing through the Parshall
161 flume. Furthermore, streamflow data from 2018 to 2019 are unavailable, and the two bimodal
162 events in 2016 were omitted from the hysteresis analysis due to substantial errors in streamflow
163 observations resulting from damage to the diversion channel. The specific observation periods are
164 detailed in Table 1. These limitations underscore the challenges associated with conducting
165 observations in remote and environmentally intricate locations.

Table 1. Rainfall-runoff event classification and counts by year. This table provides a breakdown of the number of rainfall-runoff events categorized as unimodal, bimodal, and hybrid bimodal for each year, along with the corresponding time periods. The total counts are summarized at the bottom.

Year	Unimodal event	Bimodal event	Hybrid bimodal event	Time period
Characteristics	A needle-shaped peak which responds immediately to the rainfall impulse	A delayed damped arch-shaped peak responding to the same rainfall impulse in addition to the direct peak	The delayed peak increased rapidly and merged with the direct peak, generating extremely high streamflow volume	
2014	7	-	-	Jul 25 - Sep 25
2015	12	2	-	Jun 1 - Oct 1
2016	2	2	1	Jul 10 - Aug 20
2017	-	2	-	Jun 20 - Jul 10
2020	14	2	-	Jul 1 - Oct 10
2021	15	5	2	Jun1 - Oct 10
2022	18	1	-	Apr 1 - Nov 1
2023	9	-	1	Apr 1 - Nov 1
Total	77	14	4	

2.3. Soil water content observation

Volumetric soil water content (SWC) was measured at eight observation sites using CS616 time-domain reflectometry (TDR) probes at 10-min intervals. These measurements were taken at 10-minute intervals. On Hillslope 1, five soil moisture sensors were deployed, with an additional three located adjacent to WS900. These sensors were strategically placed in the soil profiles at 80 cm depth intervals, each at a depth of 10 cm. For analysis in this study, the 10-minute interval measurements were aggregated to hourly time steps, and the arithmetic mean of the total SWC across the four profiles was employed. Moreover, SWC data immediately preceding a rainfall event were integrated over the 80 cm depth to calculate an antecedent soil moisture index (ASI), as proposed by Haga *et al.* (2005). This index, commonly utilized in analyzing the impact of

antecedent shallow soil water storage on catchment runoff response (Fu *et al.*, 2013; Penna *et al.*, 2011), provides valuable insights into the soil moisture conditions preceding rainfall events.

2.4 Groundwater level observation

Fluctuations in groundwater level (below the ground surface, hereinafter referred to as bgs) were systematically recorded in eleven 80 mm diameter boreholes situated on three hillslopes within the catchment (refer to Figure 1). The boreholes were drilled to depths of 5-26 m in granite (weathered and fractured to varying extents) mantled by thin soils. Unscreened portions of the boreholes accounted for approximately one third to three fifths of the total depth (refer to Table 2). To capture the groundwater level dynamics, HOBO capacitance water level loggers (Onset, USA) were deployed to record water levels in the boreholes at hourly intervals. It is noteworthy that water levels were rarely observed in boreholes W1-1, W1-2, W2-4, W2-5, and W2-6. This observation could be attributed to the boreholes potentially not being drilled deep enough to reach the groundwater, possibly due to challenges encountered during field drilling. Slug tests conducted following installation suggested that the saturated conductivity in the weathered and fractured granite was relatively high, ranging from 5.2×10^{-3} m/day to as high as 1.16 m/day.

Table 2. Depths and groundwater levels of boreholes. This table summarizes the depths of the bottom and the boundary between unscreened and screened portions, along with the shallowest and deepest groundwater levels of boreholes in the study area.

Borehole	Bottom (m)	Boundary (m)	Shallowest GWL (m)	Deepest GWL (m)
W1-3	10	6	2.8	10[a]
W2-1	5	2	0.2	2.2
W2-2	10	4	4.8	10[a]
W2-3	26	9	6.4	12.2
W3-1	10	4	0.8	3.9
W3-2	10	4	6.1	9.9

Note: All values indicate depths (in meters) from the ground surface; GWL represents groundwater level; 'a' indicates the groundwater level dropped below the bottom of the borehole.

An index for groundwater level (I_G) was computed by normalizing the groundwater levels in each borehole to their recorded range throughout the research years, following the approach outlined by Detty and McGuire (2010). Subsequently, the arithmetic mean of I_G across all boreholes was calculated, serving as a representative proxy for the groundwater level across the entire catchment. This approach provides a standardized measure that allows for the comparison of groundwater level variations across different boreholes within the study area.

2.5 Separation of rainfall-runoff events

An intensity-based automatic algorithm, as outlined by Tian *et al.* (2012) and Powell *et al.* (2007), was employed to delineate and segregate rainfall events from hourly rainfall time series data. In this algorithm, a threshold rainfall intensity of >0.1 mm/h was utilized to determine the commencement and conclusion of each event, with individual storms being separated by a minimum of six hours. Events characterized by an accumulated rainfall exceeding 5 mm were selected for further analysis. A total of 95 distinct rainfall events, each with a cumulative rainfall of at least 5 mm, were identified and isolated from the rainfall data series spanning the years 2014 to 2023, employing the intensity-based automatic method (refer to Table 1).

Storm runoff events are identified when streamflow experiences a rapid increase and attains a peak in response to a rain impulse. Throughout the analyses presented, streamflow refers to the total discharge measured at the weir. The computer program HYSEP (Sloto & Crouse, 1996) was employed to automatically partition a streamflow hydrograph into baseflow and stormflow components. Subsequently, the automated separation outcomes underwent manual verification and adjustment, aligning with observed data and widely accepted straight-line separation principles. In the context of each event, q_0 is defined as the streamflow before the onset of rainfall. This parameter characterizes the baseflow conditions preceding the hydrograph's response to a rain impulse (Zillgens *et al.*, 2007). The separation of stormflow from base flow allows for a more detailed examination of the runoff dynamics during distinct rainfall events.

2.6 Hydrograph and event types

The hydrograph served as a valuable tool for characterizing the timing, magnitude, and duration of runoff responses to rainfall. Two primary response types were identified based on the number and shape of streamflow peaks: unimodal and bimodal events. Schematic diagrams illustrating these three types of events are presented in Figure 2.

A unimodal event has a single peak generates during or shortly after the cessation of rain impulse (refer to Figure 2a). While a bimodal event features two peaks as a response to the same rain impulse, of which the direct peak (also called the first peak) corresponds to a fast catchment response to rainfall and occurs synchronously with the rainfall or shortly after its onset. Additionally, we referred those events has a similarly shaped hydrograph to unimodal event, but the water yield and peak delay time are significantly greater, as hybrid bimodal events. Hybrid bimodal events can be distinguished from unimodal events by their extremely high streamflow

volume, longer duration, and delayed response time (Figure 2c). The hydrographs of bimodal and hybrid bimodal events can refer to Figures 12 and 13.

It's worth noting that a rainfall event may consist of multiple impulses, and in such cases, the hydrograph responds with multiple direct peaks (see Figure 2b). The stormflows from the first peak (q_{1p}) and delayed peak (q_{2p}), along with the total event stormflow ($qs = q_{1p} + q_{2p}$), were calculated by summing hourly values over the identified event period. The runoff ratio (*Rr*), commonly used to estimate the effective contributing area during a runoff event (Buttle *et al.*, 2004; Detty & McGuire, 2010), is calculated as the ratio of *qs* to gross rainfall.

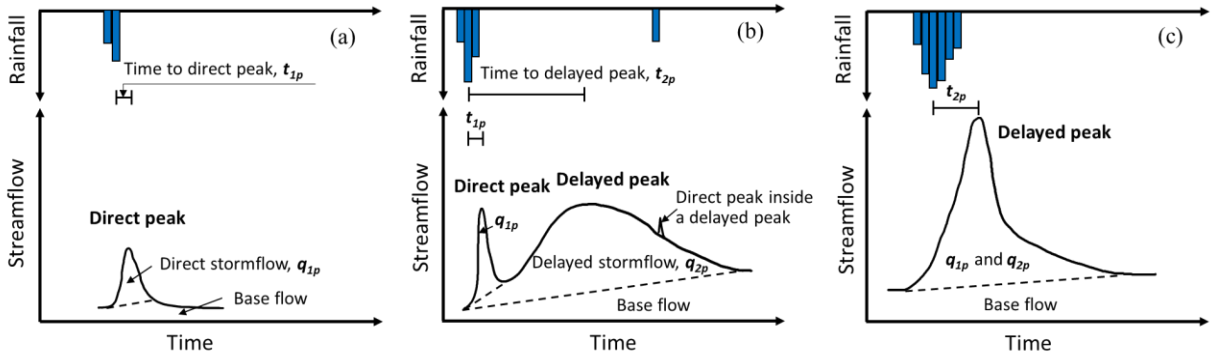

Figure 2. Schematic diagrams of the hydrographs of an (a) unimodal event, (b) typical bimodal events, and (c) hybrid bimodal event (modified from Zillgens *et al.*, 2007).

2.7 Definition of lag time

The lag time, defined as the duration between peak rainfall and peak streamflow (Mosley, 1979), is a critical parameter for modeling the temporal variability of streamflow. Lag time varies significantly among different water sources (Becker, 2005; Haga *et al.*, 2005) and has been introduced to comprehend sub-components of runoff in different response processes. In this study, two specific lag times are considered: t_{1p} the time lag between peak rainfall intensity and the first

streamflow peak, and t_{2p} the time lag between peak rainfall intensity and the delayed streamflow peak, as illustrated in Figure 2.

2.8 Water sampling and isotope analysis

Water samples for isotope analysis ($\delta^{18}O$ and δD) were collected from July 1 to September 1, 2021. Rainwater was automatically sampled every two hours using an ISCO6712 automatic water sampler (Inc., Lincoln, Nebraska, USA) positioned near the weir. Manual bulk samples of rainfall were also collected at the same location after each event using a rainwater sampler with a 9.5 cm diameter funnel attached to a 500 ml plastic water bottle, insulated with bubble foil to protect against direct sunlight, and a table tennis ball placed in the funnel's mouth to minimize evaporation.

Stream water was collected every two hours upstream of the Parshall flume location using an automatic water sampler (Figure 1). Spring, seepage water, and groundwater were manually collected daily from boreholes using a bailer. All collected samples underwent isotopic composition analysis ($\delta^{18}O$ and δD) using a Picarro L2140-i isotopic liquid water and water vapor analyzer (wavelength-scanned cavity ring-down spectroscopy, WS-CRDS) with a declared precision of $\delta^{18}O \pm 0.1‰$ and $\delta D \pm 1‰$.

2.9 Isotopic hydrograph separation

To trace the source of the streamflow during storm events, a simple mass balance approach was employed to segregate the streamflow into two components: event water and pre-event water. These components are represented by rainfall and baseflow, respectively, based on the oxygen isotopic concentration ($\delta^{18}O$) of each component. The $\delta^{18}O$ of baseflow and weighted rainwater samples served as end members, defining the ultimate isotopic composition of the stream, in accordance with the approach outlined by Padilla *et al.* (2014):

$$C_s = xC_e + (1 - x)C_p \quad (2)$$

$$x = \frac{C_s - C_p}{C_e - C_p} \cdot 100[\%] \quad (3)$$

where C_s, C_e and C_p refer to $\delta^{18}O$ concentrations of stream, event and pre-event water components, respectively. C_e is the weighted value calculated using the incremental mean weighting method (McDonnell *et al.*, 1990) for each event. C_p is determined from the stream $\delta^{18}O$ concentration measured immediately preceding the rainfall. x is the percentage of event water in stream.

3. Results

3.1 Characteristics of different runoff response types

During the period from 2014 to 2023, a total of 95 distinct rainfall events, each with a cumulative rainfall of at least 5 mm, were identified from the rainfall data series. Among these events, 14 exhibited a bimodal response, and an additional 4 displayed a hybrid bimodal process (refer to Table 1).

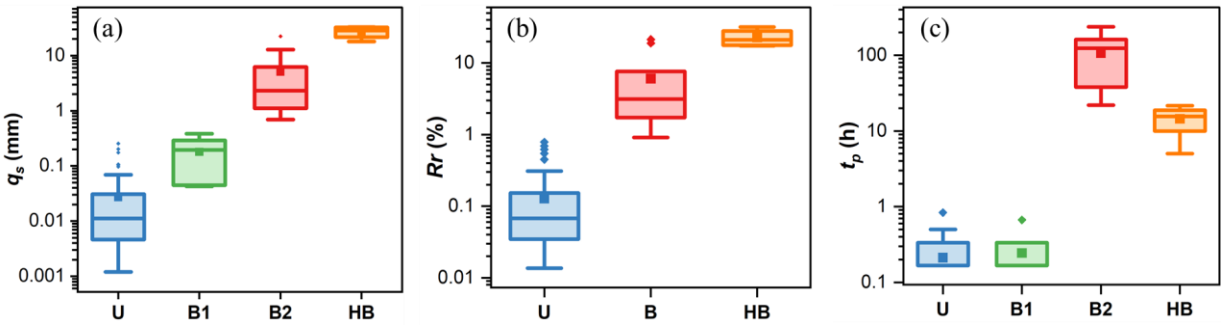

Figure 3. Comparison of (a) stormflow, q_s, (b) runoff ratio, Rr and (c) lag time (t_p) from peak rainfall to peak streamflow of different event types. U indicates unimodal event, B (including the first peak B1 and the delayed peak B2) bimodal event and HB hybrid bimodal event. In each boxplot, the lower and upper limits represent the lower and upper quartiles, while the whiskers extend to the minimum and maximum values in each dataset. The horizontal line within the box signifies the median. Individual asterisks denote points more than 1.5 times away from the median. It's noteworthy that a semi-logarithmic coordinate was utilized for enhanced interpretability due to the extensive range.

The stormflow volume and lag times of streamflow peaks for both unimodal and bimodal events were determined and characterized. As depicted in Figure 3, unimodal events generated relatively minimal runoff, with a maximum q_{1p} of 0.25 mm. In contrast, the q_{1p} and q_{2p} of bimodal events exhibited a wider range, spanning from 0.03 to 0.38 mm and from 0.82 to 31.63 mm, respectively (Figure 3b). The stormflow volume of bimodal events proved to be 3 to 114 times larger than that of unimodal events, primarily due to the presence of delayed peaks (Figure 3a). Correspondingly, bimodal events displayed higher *Rr* values ranging from 0.91% to 31.81%, whereas the *Rr* of unimodal events remained below 0.8% (Figure 3b). This discrepancy suggests an expanded effective contributing area during bimodal and hybrid bimodal events, as highlighted in previous studies (Zhang *et al.*, 2021).

In both unimodal and bimodal events, all direct peaks were observed within a one-hour timeframe. However, the delayed peak, a distinctive feature of bimodal events, manifested itself between 5 hours and 9.9 days after the occurrence of the direct peak. Notably, hybrid bimodal events exhibited shorter lag times and significantly higher stormflow yield, underscoring the need for heightened attention in flood forecasting. The substantial difference in lag time strongly implies that these peaks are contributed by distinct water sources, aligning with findings from previous studies (Haga *et al.*, 2005).

3.2 Determinants of delayed streamflow peaks

The relationships between different event types and rainfall characteristic parameters and watershed wetness indicators were further depicted in Figure 4. It is noteworthy that the soil water content (SWC) and groundwater level index (I_G) presented in Figure 4 represent data recorded at the end of rainfall events, considering that delayed streamflow peaks typically manifest subsequent to the cessation of rainfall events. Rainfall amount, I_G, and SWC were statistically significantly

different for both groups, as proven by the t-test of equality of medians at a significance level of α=0.01. The transition from unimodal to bimodal events reveals a consistent increase in rainfall amount, I_G, and SWC. Nearly all bimodal events exhibited rainfall amounts exceeding 50 mm, whereas the range for unimodal events varied from 5.2 to 66.6 mm (Figure 4a). This suggests that the initiation of delayed streamflow peaks may be associated with substantial rainfall.

The I_G and SWC of bimodal events, especially hybrid bimodal events, were significantly higher ($p < 0.01$) than those of unimodal events. Despite partial overlap in the ranges of I_G and SWC for these groups (Figure 4d and e), the mean I_G and SWC values for bimodal events (0.46 and 0.67) were notably greater than those for unimodal events (0.22 and 0.13), underscoring the distinctiveness of these parameters between event types. Contrastingly, peak rainfall intensity, mean rainfall intensity, and Antecedent Precipitation Index (API) metrics (API3, API6, and API12) exhibited a widespread overlap in their variation ($p > 0.05$, Figure 4b, d, g-i). Consequently, while bimodal events were characterized by higher rainfall and antecedent wetness, I_G and SWC emerged as more effective indicators for estimating the occurrence of bimodal events, while peak rainfall intensity, mean rainfall intensity, and API were found to be insufficient for distinguishing between bimodal and unimodal events.

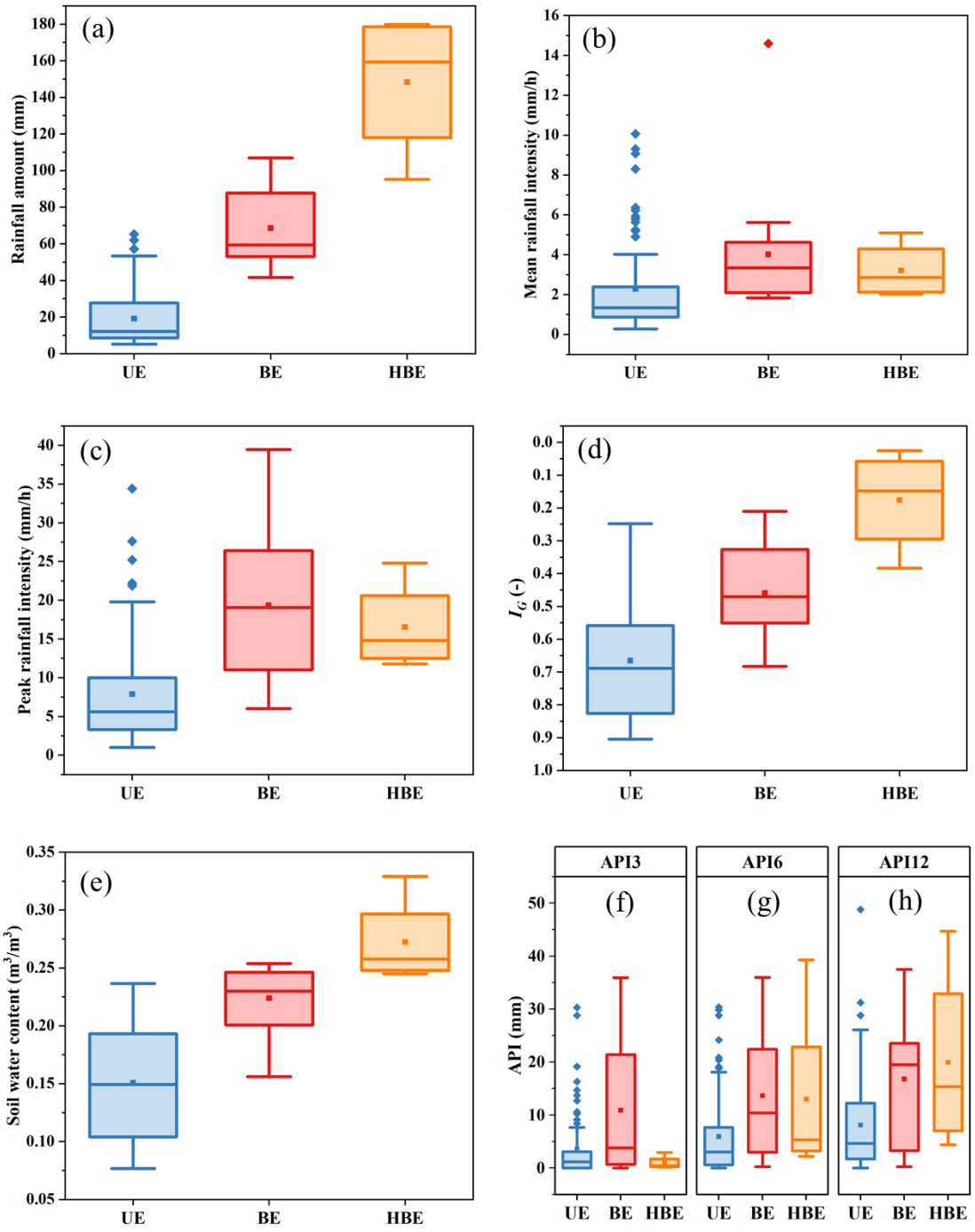

Figure 4. Box plots of the hydrological characteristic parameters for unimodal and bimodal events. (a) rainfall amount; (b) mean rainfall intensity; (c) peak rainfall intensity; (d) I_G: groundwater level index; (e) soil water content; (g)-(i) API3, API6 and API12: antecedent precipitation index over 3, 6 and 12 days. UE, BE and HBE are respectively unimodal, bimodal and hybrid bimodal events. To be noted, each element of the box carries the same interpretation as described in Figure 3.

Considering the interdependence of groundwater level, streamflow, and SWC on rainfall, a detailed examination of the relationship between rainfall amount and bimodal events was conducted. The analysis revealed that the occurrence of delayed peaks is contingent on both event rainfall and antecedent wetness, displaying a distinct threshold behavior (Figure 5b). The combined sum of event rainfall amount (P) and antecedent soil moisture index prior to the rainfall (ASI_0) serves as a reliable indicator for predicting the occurrence of delayed peaks. Figure 5 illustrates that bimodal events tend to manifest when P + ASI_0 exceeds 200 mm (with only two bimodal events misplaced). An intriguing observation is that these misplaced bimodal events produced very little q_s, and these unimodal events nearby to the threshold, occurred just before the year's first bimodal response when the watershed was sufficiently humid, signaling a predisposition for bimodal events. However, once the rainfall surpassed the threshold, all bimodal episodes were randomly distributed, and no discernible relationship was observed between their stormflow volume (q_s) and rainfall amount. Based on these findings, we posit that the stormflow generation process may be dominated by groundwater or SWC.

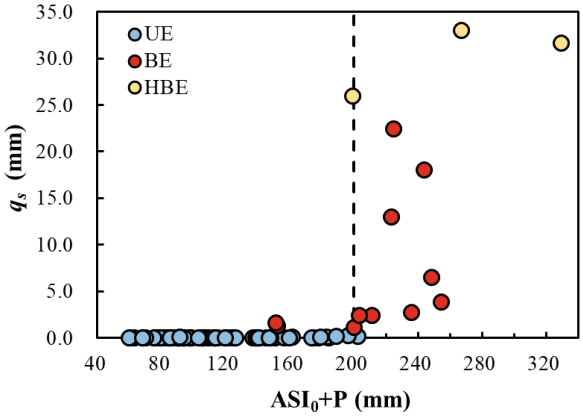

Figure 5. Relationship between the ASI_0 + P and stormflow volumes (q_s) of different event types. UE is unimodal event, HBE is hybrid bimodal event, *P* is rainfall amount, and ASI_0 is antecedent soil moisture index before the rainfall.

3.3 Timing of groundwater, soil water, and streamflow response

The preceding analysis indicates a correlation between different event types and groundwater levels along with SWC. Moreover, the inconsistent response time among different event types may signify distinct contributing sources to the stream channel, providing insights into the primary mechanisms behind runoff generation. Earlier or identical response timing of groundwater compared with streamflow suggested that streamflow response was driven by hillslope groundwater (Haught and Meerveld, 2011; Rinderer *et al*., 2016). To explore this further, six bimodal events with minimal or sporadic rainfall during the delayed peak period, along with three unimodal events, were selected. The response timing of groundwater, SWC, and streamflow is illustrated in Figure 6. Each horizontal bar represents the onset of rain on the left end and the lag time for the peak value on the right end of the corresponding variable. It's worth noting that some groundwater levels in Figures 6d, e, and g lack horizontal bars due to missing groundwater level data, while the groundwater levels in Figure 6c lack horizontal bars due to no response from groundwater.

SWC reached their maximum after direct streamflow peaks but before delayed peaks. Particularly in typical bimodal events, SWCs peaked much earlier than delayed streamflow peaks, suggesting that, in these events, soil water did not contribute to direct peak but may to delayed streamflow peaks. Regarding groundwater levels, some locations showed two peaks and not all responded to the same rainfall event. Among different locations, groundwater levels peaked before or after the delayed streamflow peaks. However, for the hybrid bimodal events, the response time of groundwater levels at various locations, and even the SWC tended to coincide with the delayed streamflow peak. Identical response timing or groundwater rising and peaking just before the stream suggest that whole catchment or critical zone contributed to delayed stormflow.

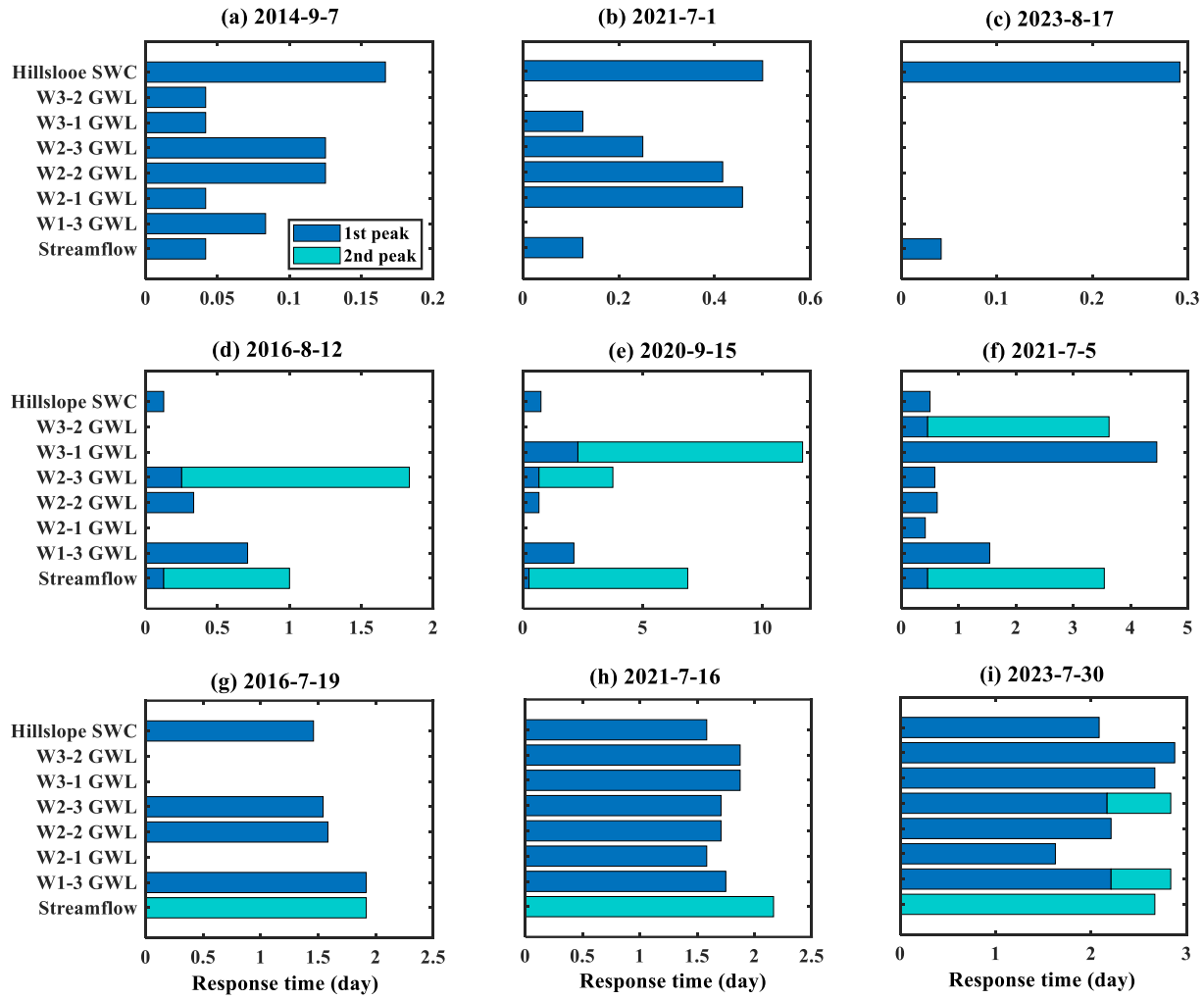

395

396 **Figure 6.** Response time of streamflow, groundwater level and soil water content in nine events.
397 The horizontal axis illustrates the lag time from the onset of rainfall. The bar lengths depict the
398 time taken for volumetric water content and groundwater level to reach their respective maximums
399 from the onset of rainfall. GWL is groundwater level, and SWC is soil water content. Each row
400 and column chart shares identical vertical and horizontal axis titles.

401 Pearson correlation coefficients (r_p) between peak groundwater levels, peak SWC and
402 delayed streamflow were calculated for 19 bimodal events. As showed in Figure 7, the first two
403 lines show the correlation coefficients between t_{2p} and the lag time of the peak groundwater levels
404 and SWC, t_{G1p} and t_{G2p} represent the response times of the first and second peaks of groundwater
405 level or SWC, respectively. The last two lines show the correlation coefficients between q_{2p} and

406 the average and peak values of groundwater levels and SWC. The number after the slash specifies
407 how many pairs of the variables.

408 Groundwater levels exhibited two peaks in some events, with the exception of W13.
409 Correspondingly, among these events, the response time of the second peak of groundwater level
410 has a strong correlation with t_{2p} with the r_p > 0.858. Even though W13's groundwater level only
411 has one peak, this peak's response time was highly correlated with t_{2p} at the 0.01 significance level
412 (r_p =0.821). In contrast, SWC displayed one peak in all events, and its response time exhibited a
413 weak correlation with t_{2p} (r_p = 0.450). Both groundwater levels and SWC, particularly their peak
414 values, demonstrated a high correlation with delayed stormflow volumes (q_s). Above all,
415 groundwater is deemed to be the primary controlling factor in delayed stormflow.

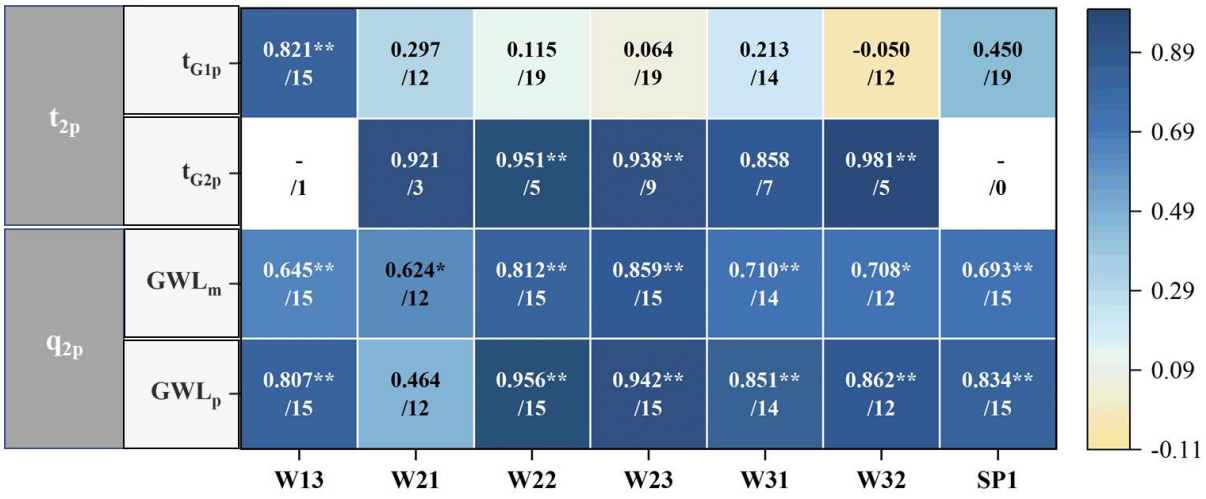

416

417 Figure 7. Pearson correlation coefficients between peak streamflow and peak groundwater levels.
418 The number after the slash specifies how many pairs of the variables. I_G, groundwater water level
419 index; ** Denotes that correlation is significant at the 0.01 level (two-tailed).
420
421 The robust correlation observed between groundwater levels at different locations and
422 stormflow suggests that groundwater observations at a specific location can serve as a
423 representative proxy for the overall groundwater level across the watershed. Given the relatively

complete and dynamic water level observation data for W23, this borehole was selected for further analysis.

3.4 Stormflow timing and magnitude characteristics

Considering the high correlation between streamflow and groundwater level as indicated in the previous analysis, we hypothesized a connection between groundwater and delayed stormflow. To elucidate this correlation between groundwater and streamflow, we fitted the relationship between the groundwater level at location W23 and the magnitude and timing of the delayed stormflow for bimodal events. The time lag of delayed peak (t_{2p}) shows a negative exponential correlation with peak groundwater level ($ln(t_{2p}) = 1.03 \times PGL - 7.43$, $R^2 = 0.84$, $p < 0.01$, Figure 8), suggesting that a higher groundwater level corresponds to a faster response of the delayed runoff peak to rainfall. A comparable linear correlation was also fitted between t_{2p} and groundwater level, albeit with a slightly lower R^2 ($R^2 = 0.76$).

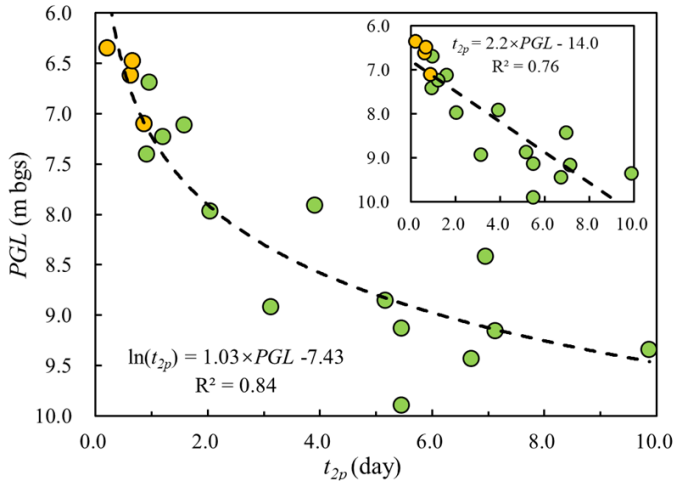

Figure 8. Correlation between peak groundwater level (*PGL*) and lag time of the delayed streamflow peak (t_{2p}). The insert shows the same plot with linear fitting. Orange solid circles represent hybrid bimodal events.

Moreover, as shown in Figure 9, q_s also has a strong linear relationship with groundwater level ($q_s = -10 \times PGL + 94.8$, $R^2 = 0.91$, $p < 0.01$). These results highlight the significant influence

of groundwater on flood generation in the studied watershed, suggesting that incorporating groundwater level variations into flood forecasting models could enhance their accuracy.

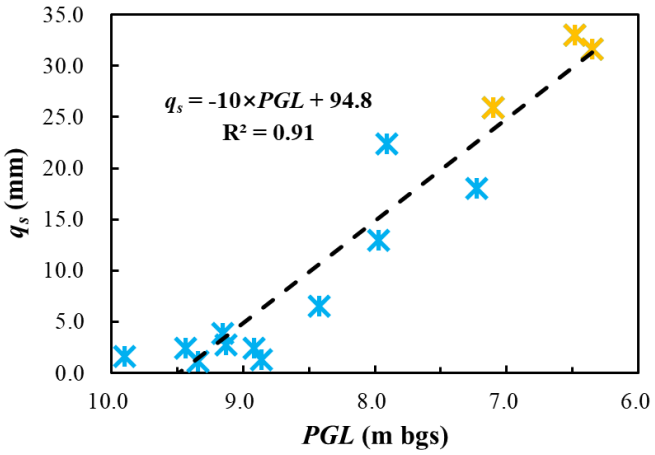

Figure 9. Correlation between peak groundwater (*PGL*) level and stormflow amount (q_s) for bimodal events. Orange stars represent hybrid bimodal events.

For both fitted lines, the closely matching fitting lines for hybrid bimodal events support the hypothesis that these high, delayed streamflow responses, which may appear unimodal, are, in fact, bimodal. During hybrid bimodal events, the delayed peak increased rapidly and reached its peak within one day, practically merging with the direct peak. This led to a potentially misleading result that only one peak was generated. This occurrence was likely due to the groundwater level rising rapidly to a critical level with substantially higher hydraulic conductivity, allowing a larger portion of the hillslope to become hydraulically connected to the stream during these events within a very short time. Consequently, a substantial amount of groundwater was quickly discharged into the channel.

3.5 Isotope composition of groundwater and stream water

To gain additional insight into the control of groundwater level on delayed stormflow, the isotope compositions of different water bodies were analyzed. Figure 10 summarizes the $\delta^{18}O$ of stream, spring, seepage water and the groundwater $\delta^{18}O$ from all boreholes between July 1 and

September 1 in 2021. Rainwater exhibited a high variation in $\delta^{18}O$ composition (ranging from -14.42 to -5.28 ‰), with a rainfall-weighted mean $\delta^{18}O$ value of -9.197. In contrast, groundwater $\delta^{18}O$ composition appeared more stable throughout the sampling period, showing little variation across various boreholes, with a mean $\delta^{18}O$ value ranging from -9.76±0.10 to -9.08±0.86‰. This stability indicates minimal event-based mixing with rainwater. The $\delta^{18}O$ values of spring and seepage water followed a pattern similar to that of groundwater. The average $\delta^{18}O$ value of the stream (-9.51‰) closely resembled that of groundwater (-9.49‰). Although the stream's $\delta^{18}O$ composition briefly deviated toward that of rainfall during a storm, it quickly reverted to its previous value, resembling groundwater. Large isotopic variation in rainfall was dampened in the stream, indicating that both baseflow and some stormflow originated from groundwater storage with a consistent isotopic ratio, a result of dispersion and mixing processes.

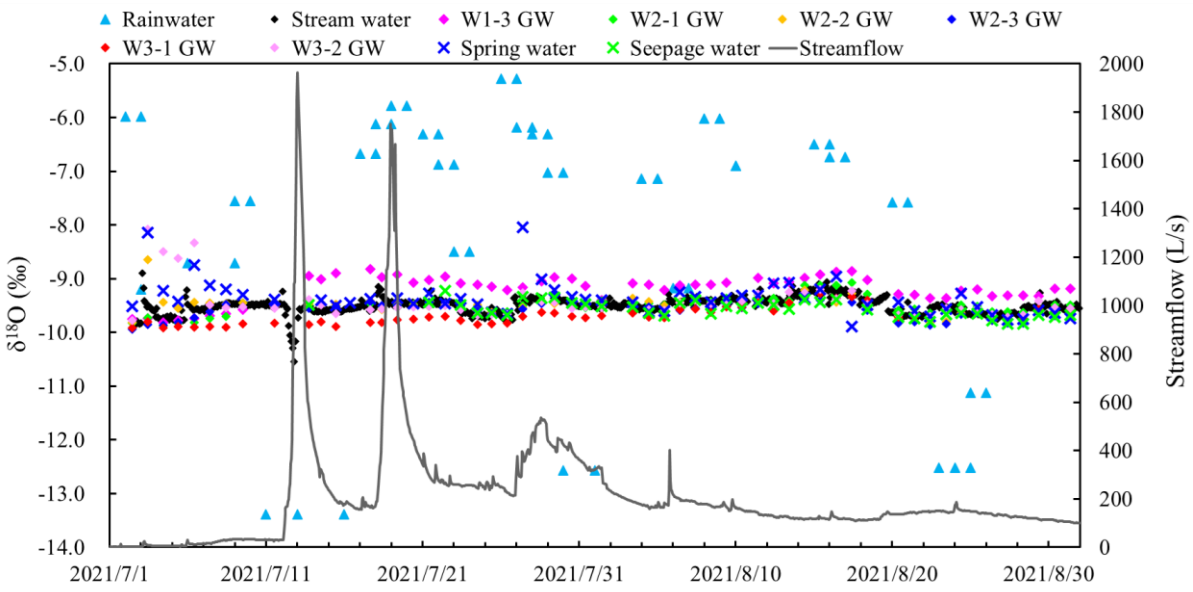

Figure. 10. Stable isotope $\delta^{18}O$ time series of rainwater, stream water and groundwater.

In Figure 11, groundwater $\delta^{18}O$ values were plotted against groundwater levels for each borehole, and stream water $\delta^{18}O$ values were plotted against streamflow. The variability of groundwater $\delta^{18}O$ increased with rising groundwater levels, suggesting a stronger influence of

rainwater on groundwater. Stream water's $\delta^{18}O$ remained independent of streamflow volume and exhibited a range of variation similar to that of groundwater. Notably, the overlapping isotopic compositions, including those during stormflow, were predominantly found in regions with higher groundwater levels. This observation underscores that, even during stormflow events, groundwater remains the primary source of streamflow.

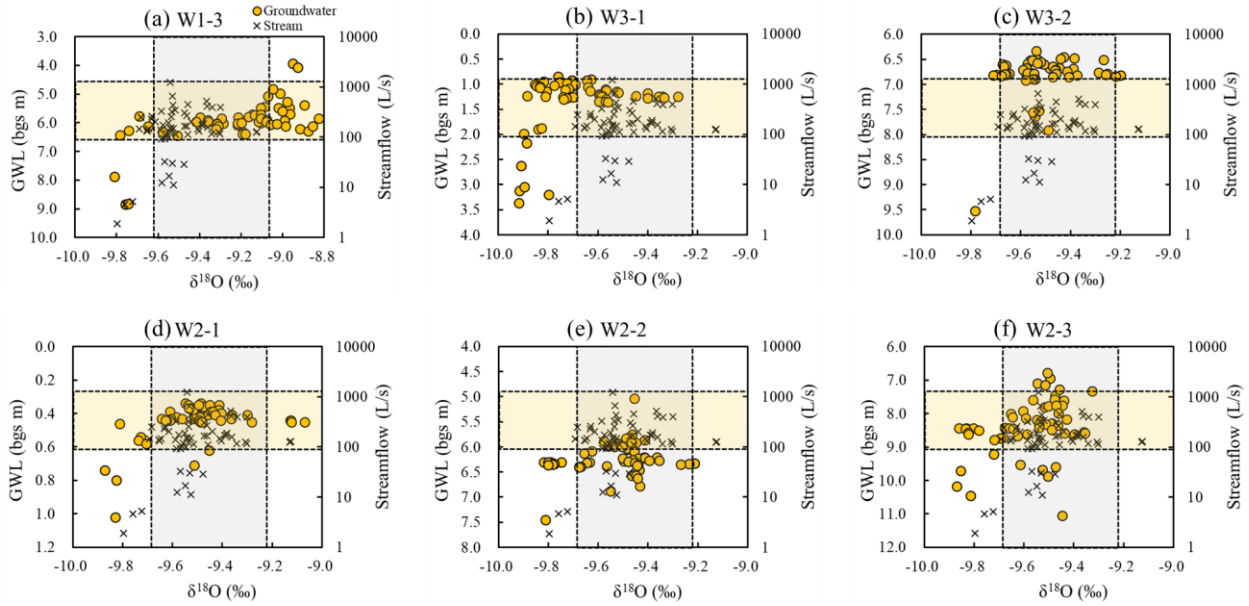

Figure 11. $\delta^{18}O$ measurements in groundwater and stream water from July 1 to September 1, 2021. Circles and cross represent the $\delta^{18}O$ of groundwater and stream water, respectively.

4. Discussion

4.1 Lag time of delayed streamflow peaks

The lag time of delayed peaks varies across different water sources, providing valuable insights for estimating stormflow water resources. Haga *et al.* (2005) conducted relevant studies in a forested unchanneled catchment, noting that events with shorter lag times (<2 hours) predominantly exhibited runoff composed of saturation excess overland flow near the spring area. In contrast, events with longer lag times (>24 hours) were characterized by river runoff mainly

composed of saturated subsurface flow above the soil-bedrock interface. Becker (2005) synthesized lag times from various studies in different basins, observing a trend where lag times for the three main flow components differed by at least one order of magnitude, following the pattern overland flow < subsurface flow < baseflow. This substantial difference in lag times is likely attributed to the stochastic triggering of different flow paths by rainfall forcing in distinct events.

Lag times for the direct streamflow peaks, observed in both unimodal and bimodal events in this study, were generally within 30 minutes. These lag times exhibited no significant correlation with rainfall amount, rainfall intensity, or pre-event streamflow (correlation coefficients of 0.005, 0.017, and 0.012, respectively). This lack of correlation suggests that the direct streamflow peaks were nearly concurrent with rainfall. Therefore, we infer that these direct peaks were generated either through bypass flow mechanisms, such as macropores, fractures, or soil-bedrock interfaces, as interpreted in Buttle and Turcotte (1999), Onda *et al.* (2001), Uchida *et al.* (2005), and Xu *et al.* (2016). Alternatively, they could have been directly contributed to the channel by rainfall. This interpretation aligns with the consideration that the routing time of the river network in XEW is approximately 1 hour (Zhao *et al.*, 2019).

In contrast to the direct peaks, the time lags from the peak rainfalls to the delayed peaks were considerably longer, ranging from 5 hours to 9.9 days (Figure 3). This lag time in our study aligns with findings from other studies where similar parameters were calculated (refer to Table 3). The results imply that the delayed peaks observed in XEW were likely generated by subsurface flow processes, as indicated in the work of Lischeid *et al.* (2002).

514 **Table 3.** Lag time between peak rainfall intensity and the delayed streamflow peak in this study
515 and in previous studies.

Reference	Lag time of delayed peak	The source of the delayed peak
Anderson & Burt (1978)	About one day	Subsurface flow
Onda *et al.* (2001)	Ten hours to one week	Subsurface flow and bedrock groundwater
Masiyandima *et al.* (2003)	Several hours	Subsurface flow
Becker (2005)	A day to several weeks	Subsurface stormflow
Zillgens *et al.* (2007)	Three to five days	Subsurface flow
Birkinshaw (2008)	Several tens of hours to a few days	Subsurface stormflow
Kosugi *et al.* (2011)	Two to three days	Bedrock groundwater
Fenicia *et al.* (2014)	Several hours or days	Subsurface flow
Padilla *et al.* (2014, 2015)	Within four days	Bedrock groundwater
Yang *et al.* (2015)	Several hours	Subsurface flow
This study	5 hours to 9.9 days	Subsurface flow (groundwater flow)

516

517 **4.2 Hysteresis between groundwater level and streamflow**

518 For bimodal events in XEW, the non-linear relationship between groundwater level and
519 streamflow results in hysteretic relationships between the two variables. Figure 12 shows time
520 series for streamflow and I_G as well as scatter plots comparing the two variables for the six events
521 used in section 3.3. As noted by Dunne (1978), when two runoff peaks appeared in an event, there
522 must be at least two zones in the catchment that responded to the storm and contributed to runoff.
523 The hysteretic nature highlights the possibility of multiple hydrological compartments being active

524 and these compartments are not necessarily contributing significant flows simultaneously but
525 rather sequentially during the runoff generation period (Fovet *et al.*, 2015; Martínez-Carreras *et*
526 *al.*, 2016).
527
528

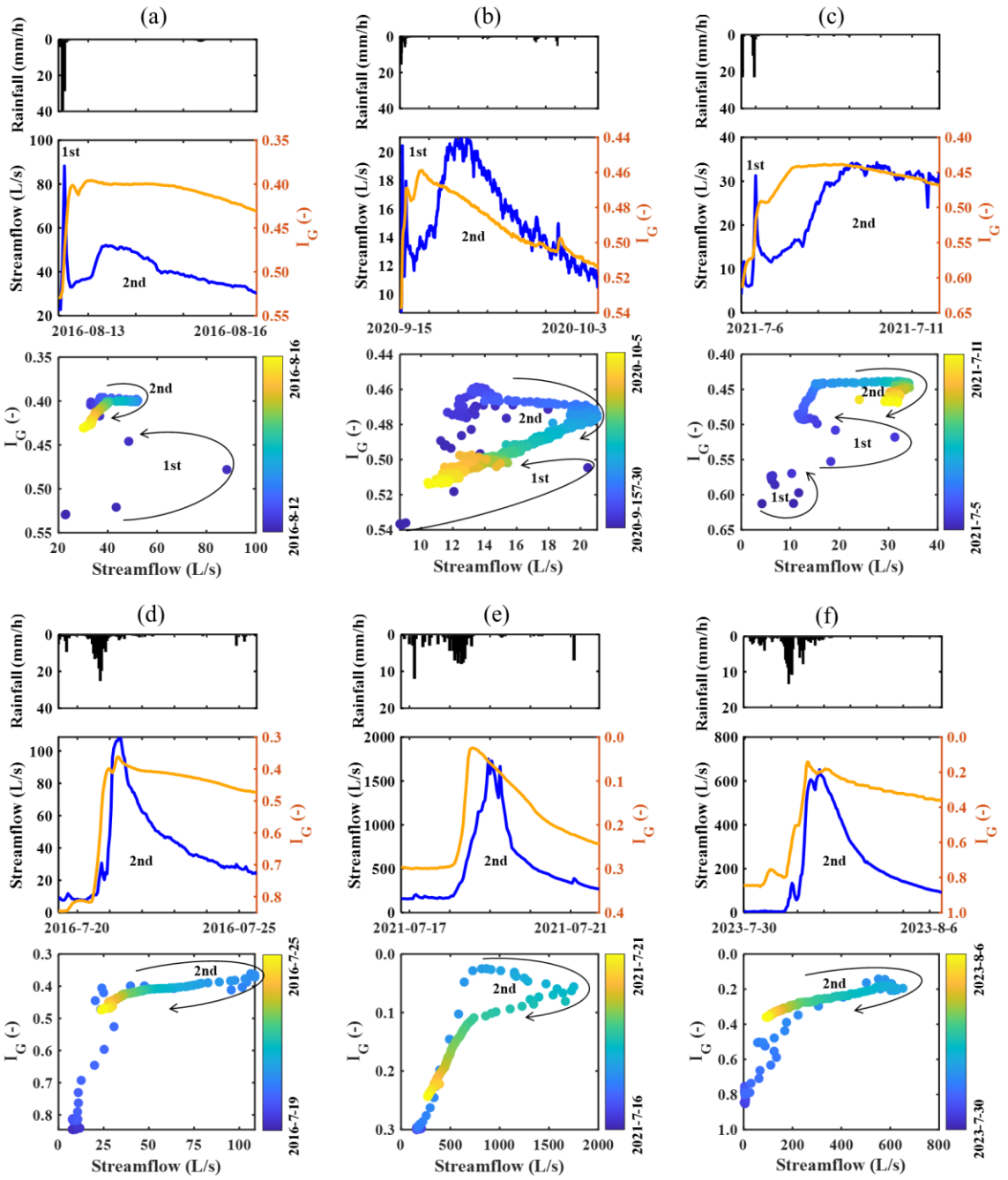

Figure 12. Streamflow and I_G with corresponding scatter plots between both variables for three typical bimodal and three hybrid bimodal events. Note that the axis scales vary between events. Arrows indicate progression of time. Direct peaks in bimodal hydrographs indicated as "1st" and delayed peaks as "2nd".

Streamflow increased quickly and peaked before groundwater level during direct peaks, resulting in an anti-clockwise hysteretic loop. It can be explained that direct peaks were formed by rainfall directly falling onto the channel or a saturation zone near the channel, and/or by the flow that contributed to the channel through rapid routes, as observed in other watersheds by Jackisch *et al.* (2016). In contrast, groundwater level peaked first during delayed peaks, indicating that the groundwater level in the watershed peaked first and subsequently released water, creating the delayed runoff peak. This behavior may be attributed to the groundwater level surpassing a threshold for generating bimodal hydrographs, leading to enhanced hydraulic connectivity between hillslopes and the channel. This, in turn, resulted in the swift release of a substantial amount of groundwater or subsurface flow (Burt & Butcher, 1985; Detty and McGuire, 2010; McGlynn & McDonnell, 2003; McGuire and McDonnell, 2010; Scaife and Band, 2017). Consequently, the groundwater level is not merely a passive feature in this watershed, where shallow groundwater may constitute the primary runoff component, but actively controls the stormflow.

4.3 Two-component hydrograph separation

The two-component hydrograph separation was performed for four bimodal storm events using the $\delta^{18}O$ of the bulk rainfall, a pre-event water signature (represented by the stream $\delta^{18}O$ before the rainfall) and the monitored stream water signature during the events. These four events were chosen because their relatively complete isotope data. It should be noted that in all four rainfall events, $\delta^{18}O$ values in rain and stream water were notably different, which is a requirement for end-member hydrograph separation analysis. The hydrograph separation results, as well as the $\delta^{18}O$ series of rainwater and stream water were shown in Figure 13.

Regarding the water sources separation result, these four events can be divided into two groups: Event B1 and B4, the major stormflow process were lagged and considerably damped, and event water contributions were higher compared to the other two events. The fraction of event water comprising the hydrograph was 25% in Event B1, and the contribution ratio of event water in Event 4 was 11%. Considering that the rain had already stopped, the event water component of the delayed peak should be the rainwater temporarily stored in the watershed during the rainfall process. Event B2 and especially Event B3, however, were almost entirely pre-event water dominated (the contributions of pre-event water were 92% for Event 2 and 97% for Event B3), although it was evident that some event water contributed to the stormflow during the rising and peak period of streamflow, this water may have originated from the direct rainfall or rain water taking a rapid route to the stream channel.

The hydrograph separation results indicated that the streamflow contribution of pre-event water changed virtually in sync with streamflow following the onset of rain, almost entirely dominating the hydrograph, while event water dominated the sharp streamflow peak responding to high-intensity storm. Early in the rainy event, the pre-event component of the hydrograph exceeded 50%, indicating a sufficiently swift groundwater response such that considerable amounts of groundwater were released soon after the start of rain.

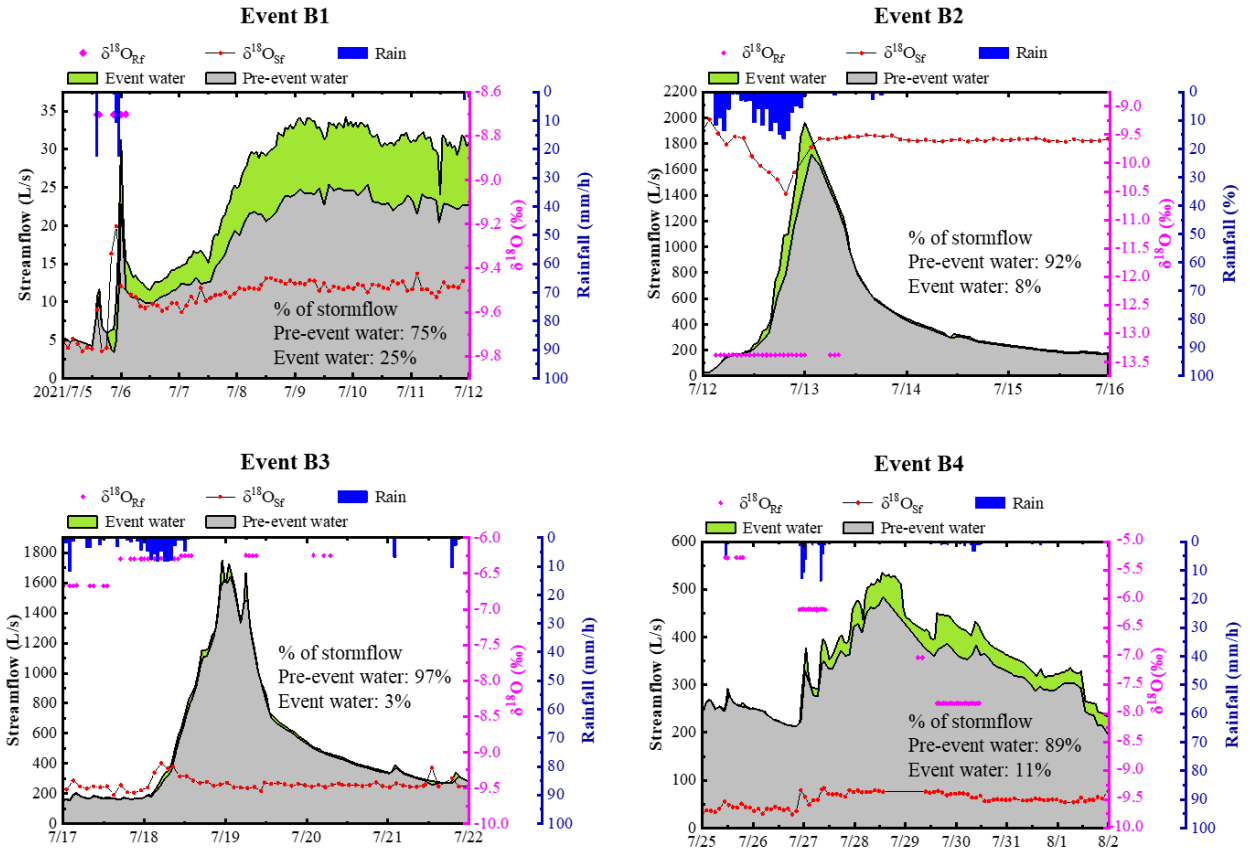

Figure 13. The partitioning of stormflow into its pre-event and event water sources using one-tracer two component hydrograph separation analysis with $\delta^{18}O$ as tracer for the four storm events. $\delta^{18}O_{Rf}$ and $\delta^{18}O_{Sf}$ are the $\delta^{18}O$ respectively for rain and stream water.

In addition, there was a noticeable, gradual rise in the pre-event water contribution to total stormflow as the catchment was wetting-up (Figure 13). Event B1 had a rather dry antecedent condition and showed a relatively lower pre-event water percentage (about 75%). Event 3 in the temporal sequence had a extremely high pre-event water proportion (approximately 97%) and occurred under highly wet antecedent conditions. In Event B4, due to a little reduced wetness condition compared to the preceding Event B3, the percentage of pre-event water decreased somewhat to approximately 89%. This pattern may be attributed to increased water flux during the wetting-up process when the water table rose into near surface soil layers with high saturated hydraulic conductivity. The rate of groundwater increase slowed as a result of the higher

transmissivity, and more pre-event water was mobilized and travelled rapidly to the stream via shallow flow pathways (Lundin, 1982).

4.4 Filed observation

Our field observations on-site indicate that direct exfiltration of groundwater into the runoff predominates, with few signs of hillslope overland flow. For example, during a heavy storm on July 5, 2021, characterized by short duration (7 hours) and very high intensity (27.6 mm/h) with a total rainfall of 65.2 mm, minimal overland flow was observed at the study site. However, post the storm on July 5, the spring water flow from Hillslope 2 substantially increased. Moreover, at various points in the watershed, seepage flow was observed gushing from fractures in the stone and holes in the earth. These field observations strongly suggest the direct exfiltration of groundwater into the runoff, providing further support to the notion that groundwater significantly contributes to stormflow in the watershed.

Figure 14. Field observations of the spring and the seepage flows. HS1, HS2 and HS3 are Hillslope 1, Hillslope 2 and Hillslope 3, respectively.

5. Conclusions

Based on observations from 2013 to 2023, the study carried out an event-scale analysis of streamflow hydrographs in a semi-humid forested watershed of North China. Three stormflow

patterns with distinct shaped hydrograph, i.e., unimodal, bimodal, and hybrid bimodal were identified. Particularly, their rainfall-runoff response characteristics as well the stormflow composition were analyzed, and derived the following conclusions:

1) Direct peaks for both unimodal and bimodal events occurred within 1 hour following the peak rainfall, while the lag time of delayed peaks ranged between 5 h and 9.9 days. The stormflow amount generated by bimodal events, due to the delayed peak, was several to hundreds of times more than that of the unimodal events, often resulting in flooding.

2) Delayed stormflow appeared when the sum of event rainfall amount (P) and antecedent soil moisture index (ASI) exceeding 200 mm. Stormflow yield is positively proportional to event peak groundwater level while the lag time of delayed peak showed an inverse correlation with peak groundwater level.

3) The isotopic analysis and two-component hydrograph separation unveiled that pre-event water predominantly contributed to the delayed stormflow, with event water dominating the sharp streamflow peak in response to high-intensity storms.

4) Streamflow peaked before groundwater level during direct peaks, suggesting that direct streamflow peaks are from direct rainfall onto the channel or rapid flow through macropores and bedrock fractures, Discharge peaked before catchment storage during single peak. But groundwater levels peaked first during delayed streamflow, suggested that the delayed stormflow is primarily made up of shallow groundwater, and this is further supported by field observation.

This study clarified the prerequisites for bimodal stormflow, and the provided information on the response characteristics and water resources of stormflow is not common knowledge for regions. We believe these findings can enrich runoff generation theory and contribute new insights for stormflow modelling in other similar regions.

Data availability

All the data used in this study will be available at the Zenodo website at the time of publication.

Author contribution

ZC contributed the conceptualization, formal analysis, investigation and writing; FT contributed the conceptualization, formal analysis and revision; ZZ, ZX, YD and JW contributed the Investigation; M contributed the writing.

Competing interests

Some authors are members of the editorial board of Hydrology and Earth System Sciences.

Financial support

This study was supported by the National Key R&D Program of China (2022YFC3002902) and the National Natural Science Foundation of China (51825902).

Acknowledgments

We acknowledge Jeffrey McDonnell for constructive advice on this study.

References

Ali, G., Tetzlaff, D., McDonnell, J. J., Soulsby, C., Carey, S., Laudon, H., McGuire, K., Buttle, J., Seibert, J., Shanley, J. (2015). Comparison of threshold hydrologic response across northern catchments. *Hydrological Process*, *29 (16)*, 3575–3591. https://doi.org/10.1002/hyp.10527

Anderson, M. G., & Burt, T. P. (1977). Automatic monitoring of soil moisture conditions in a hillslope spur and hollow. *Journal of Hydrology*, *33*(1–2), 0–36. https://doi.org/10.1016/0022-1694(77)90096-8

Anderson, M. G., & Burt, T. R. (1978). The role of topography in controlling throughflow generation. *Earth Surface Processes*, *3*(4), 331–334. https://doi.org/10.1002/esp.3290030402

Becker, A. (2005). Runoff Processes in Mountain Headwater Catchments: Recent Understanding and Research Challenges. *Global Change and Mountain Regions*, 283–295. https://doi.org/10.1007/1-4020-3508-x_29

Becker, A., & Mcdonnell, J. J. (1998). Topographical and ecological controls of runoff generation and lateral flows in mountain catchments. *IAHS Publications-Series of Proceedings and Reports-Intern Assoc Hydrological Sciences*, *248*, 199-206.

Birkinshaw, S. J. (2008). Physically ‐ based modelling of double ‐ peak discharge responses at Slapton Wood catchment. *Hydrological Processes: An International Journal*, *22*(10), 1419–1430. https://doi.org/10.1002/hyp.6694

Burt, T. P., & Butcher, D. P. (1985). Topographic controls of soil moisture distributions. *Journal of Soil Science*, *36*(3), 469–486. https://doi.org/10.1111/j.1365-2389.1985.tb00351.x

Buttle, J. M., Dillon, P. J., & Eerkes, G. R. (2004). Hydrologic coupling of slopes, riparian zones and streams: An example from the Canadian Shield, *Journal of Hydrology*, *287*(1–4), 161–177. https://doi.org/10.1016/j.jhydrol.2003.09.022

Buttle, J. M., & Turcotte, D. S. (1999). Runoff processes on a forested slope on the Canadian Shield. *Hydrology Research*, *30*(1), 1-20. https://doi.org/10.1016/S0304-2995(99)80027-8

Detty, J. M., & Mcguire, R. J. (2010). Threshold changes in storm runoff generation at a till-mantled headwater catchment. *Water Resources Research*, *46*(7), 759–768. https://doi.org/10.1029/2009wr008102

Dingman, S. L. (2015). Physical hydrology. Long Grove, IL: Waveland Press.

Dubreuil, P. L. (1960). Etude hydrologique de petits bassins en Cote d'Ivoire. Rapport general. ORSTOM Service Hydrologique.

Dubreuil, P. L. (1985). Review of field observations of runoff generation in the tropics. *Journal of Hydrology*, *80(3-4)*, 237–264. https://doi.org/10.1016/0022-1694(85)90119-2

673 Dunne, T. (1978). Field studies of hillslope flow processes. In M. J. Kirkby (Eds.), Hillslope Hydrology (pp.
674 227–293). London, Wiley.
675 Fenicia, F., Kavetski, D., Savenije, H. H., Clark, M. P., Schoups, G., Pfister, L., & Freer, J. (2014). Catchment
676 properties, function, and conceptual model representation: is there a correspondence?. Hydrological
677 Processes, *28*(4), 2451-2467. https://doi.org/10.1002/hyp.9726
678 Fovet, O., Ruiz, L., Hrachowitz, M., Faucheux, M., & Gascuel-Odoux, C. (2015). Hydrological hysteresis and
679 its value for assessing process consistency in catchment conceptual models. *Hydrology and Earth System*
680 *Sciences*, *19*(1), 105-123. https://doi.org/10.5194/hess-19-105-2015
681 Fu, C., Chen, J., Jiang, H., & Dong, L. (2013). Threshold behavior in a fissured granitic catchment in southern
682 China: 1. Analysis of field monitoring results. *Water Resources Research, 49(5),* 2519–2535.
683 https://doi.org/10.1002/wrcr.20191
684 Graeff, T., Zehe, E., Reusser, D., Lück, E., Schröder, B., Wenk, G., John, H., & Bronstert, A. (2009). Process
685 identification through rejection of model structures in a mid-mountainous rural catchment: observations of
686 rainfall-runoff response, geophysical conditions and model inter-comparison. *Hydrological Processes*,
687 *23*(5), 702–718. https://doi.org/10.1002/hyp.7171
688 Gu, W. (1996). On the hydrograph separation traced by environmental isotopes. *Advances in Water Science*,
689 *7*(2): 105–111.
690 Haga, H., Matsumoto, Y., Matsutani, J., Fujita, M., Nishida, K., & Sakamoto, Y. (2005). Flow paths, rainfall
691 properties, and antecedent soil moisture controlling lags to peak discharge in a granitic unchanneled
692 catchment. *Water Resources Research, 41*(12), 2179–2187. https://doi.org/10.1029/2005wr004236
693 Iwagami, S., Tsujimura, M., Onda, Y., Shimada, J., & Tanaka, T. (2010). Role of bedrock groundwater in the
694 rainfall-runoff process in a small headwater catchment underlain by volcanic rock. *Hydrological Processes*,
695 *24*(19), 2771–2783. https://doi.org/10.1002/hyp.7690
696 Jackisch, C., Angermann, L., Allroggen, N., Sprenger, M., Blume, T., Weiler, M., Tronicke, J., & Zehe, E.
697 (2016). In situ investigation of rapid subsurface flow: identification of relevant spatial structures beyond

heterogeneity. *Hydrology and Earth System Sciences Discussions*, 1–32. https://doi.org/10.5194/hess-2016-190

Jenkins, A., Ferrier, R. C., Harriman, R., & Ogunkoya, Y. O. (1994). A case study in catchment hydrochemistry: Conflicting interpretations from hydrological and chemical observations, *Hydrological Processes*, *8*(4), 335–349. https://doi.org/10.1002/hyp.3360080406

Kosugi, K., Fujimoto, M., Katsura, S., Kato, H., Sando, Y., & Mizuyama, T. (2011). Localized bedrock aquifer distribution explains discharge from a headwater catchment. *Water Resources Research*, *47(7)*. https://doi.org/1029/2010WR009884

Lischeid, G., Kolb, A., & Alewell, C. (2002). Apparent translatory flow in groundwater recharge and runoff generation. *Journal of Hydrology*, *265*(1–4), 195–211. https://doi.org/10.1016/s0022-1694(02)00108-7

Lundin L. (1982) Soil moisture and ground water in till soil and the significance of soil type for runoff. PhD Thesis, Uppsala University, UNGI Report, 56, 216.

Martínez-Carreras, N., Hissler, C., Gourdol, L., Klaus, J., Juilleret, J., Iffly, J. F., & Pfisteret, L. (2016). Storage controls on the generation of double peak hydrographs in a forested headwater catchment. *Journal of Hydrology*, *543*, 255–269. https://doi.org/10.1016/j.jhydrol.2016.10.004

Martínez-Carreras, N., Wetzel, C. E., Frentress, J., Ector, L., McDonnell, J. J., Hoffmann, L., Pfister, L., 2015. Hydrological connectivity inferred from diatom transport through the riparian-stream system. *Hydrology and Earth System Sciences*, *19*(7), 3133–3151. https://doi.org/10.5194/hess-19-3133-2015

Masiyandima, M. C., van de Giesen, N., Diatta, S., Windmeijer, P. N., & Steenhuis, T. S. (2003). The hydrology of inland valleys in the sub-humid zone of West Africa: rainfall-runoff processes in the M'be experimental watershed. *Hydrological Processes*, *17*(6), 1213–1225. https://doi:10.1002/hyp.1191

McDonnell, J. J., Bonell, M., Stewart, M. K., & Pearce, A. J. (1990). Deuterium variations in storm rainfall: Implications for stream hydrograph separation. *Water resources research*, *26*(3), 455-458. https://doi.org/10.1029/WR026i003p00455

McDonnell, J. J., Sivapalan, M., Vaché, K., Dunn, S., Grant, G., Haggerty, R., Hinz, C., Hooper, R., Kirchner, J., Roderick, M. L., Selker, J., Weiler, M. (2007). Moving beyond heterogeneity and process complexity:

A new vision for watershed hydrology. *Water Resources Research*, *43(7)*. https://doi.org/10.1029/2006WR005467

McGlynn, B. L., & McDonnell, J. J. (2003). Quantifying the relative contributions of riparian and hillslope zones to catchment runoff, *Water Resources Research*, *39(11)*, 1310. https://doi.org/10.1029/2003wr002091

McGuire, K. J., & McDonnell, J. J. (2010). Hydrological connectivity of hillslopes and streams: Characteristic time scales and nonlinearities. *Water Resources Research*, *46(10)*. https://doi.org/10.1029/2010WR009341

Mosley, M. P. (1979). Streamflow generation in a forested watershed, New Zealand. *Water Resources Research*, *15*(4), 795–806. https://doi.org/10.1029/wr015i004p00795

Onda, Y., Komatsu, Y., Tsujimura, M., & Fujihara, J. (2001). The role of subsurface runoff through bedrock on storm flow generation. *Hydrological Processes*, *15*(10), 1693–1706. https://doi.org/10.1002/hyp.234

Padilla, C., Onda, Y., Iida, T., Takahashi, S., & Uchida, T. (2014). Characterization of the groundwater response to rainfall on a hillslope with fractured bedrock by creep deformation and its implication for the generation of deep-seated landslides on Mt. Wanitsuka, Kyushu Island. *Geomorphology*, *204*, 444–458. https://doi.org/10.1016/j.geomorph.2013.08.024

Padilla, C., Onda, Y., & Iida, T. (2015). Interaction between runoff-bedrock groundwater in a steep headwater catchment underlain by sedimentary bedrock fractured by gravitational deformation. *Hydrological Processes*, *29*(20), 4398–4412. https://doi.org/10.1002/hyp.10498

Penna, D., Tromp-van Meerveld, H. J., Gobbi, A., Borga, M., & Dalla Fontana, G. (2011). The influence of soil moisture on threshold runoff generation processes in an alpine headwater catchment. *Hydrology and Earth System Sciences*, *15(3)*, 689–702. https://doi.org/10.5194/hess-15-689-2011

Phillips, J. D. (2003). Sources of nonlinearity and complexity in geomorphic systems, *Progress in Physical Geography*, *27(1)*, 1–23. https://doi.org/10.1191/0309133303pp340ra

Powell, D. N., Khan, A. A., Aziz, N. M., & Raiford, J. P. (2007). Dimensionless rainfall patterns for South Carolina. *Journal of Hydrologic Engineering*, *12(1)*, 130–133. https://doi.org/10.1061/(asce)1084-0699(2007)12:1(130)

Ross, C. A., Ali, G. A., Spence, C., & Courchesne, F. (2021). Evaluating the Ubiquity of Thresholds in Rainfall - Runoff Response Across Contrasting Environments. *Water Resources Research, 57(1)*, e2020WR027498. https://doi.org/10.1029/2020wr027498

Scaife, C. I., & Band, L. E. (2017). Nonstationarity in threshold response of stormflow in southern Appalachian headwater catchments. *Water Resources Research*, *53(8)*, 6579–6596. https://doi.org/10.1002/2017WR020376

Sivapalan, M. (2003), Process complexity at hillslope scale, process simplicity at the watershed scale: Is there a connection? *Hydrol. Processes*, *17(5)*, 1037–1041. https://doi:10.1002/hyp.5109.

Sloto, R. A., & Crouse, M. Y. (1996). HYSEP: A computer program for streamflow hydrograph separation and analysis (No. 96-4040). US Geological Survey. https://doi.org/10.3133/wri964040

Tian, F., Li, H., & Sivapalan, M. (2012). Model diagnostic analysis of seasonal switching of runoff generation mechanisms in the blue river basin, oklahoma. *Journal of Hydrology*, *418–419*, 136–149. https://doi.org/10.1016/j.jhydrol.2010.03.011

Tie, Q., Hu, H., Tian, F., Guan, H., & Lin, H. (2017). Environmental and physiological controls on sap flow in a subhumid mountainous catchment in north china. *Agricultural and Forest Meteorology*, *240–241*, 46–57. https://doi.org/10.1016/j.agrformet.2017.03.018

Tromp-van Meerveld, H. J., & McDonnell, J. J. (2006), Threshold relations in subsurface stormflow: 1. A 147-storm analysis of the Panola hillslope. *Water Resources Research, 42*, W02410. https://doi.org/10.1029/2004WR003778

Uchida, T., Tromp-van Meerveld, I., & McDonnell, J. J. (2005). The role of lateral pipe flow in hillslope runoff response: An intercomparison of non-linear hillslope response. *Journal of Hydrology*, *311(1-4)*, 117–133. https://doi.org/10.1016/j.jhydrol.2005.01.012

Westhoff, M. C., Bogaard, T. A., & Savenije, H. H. G. (2011). Quantifying spatial and temporal discharge dynamics of an event in a first order stream, using distributed temperature sensing. *Hydrology and Earth System Sciences*, *15*(6), 1945-1957. https://doi.org/10.5194/hess-15-1945-2011

774 Weyman, D., R. (1970). Throughflow on hillslopes and its relation to the stream hydrograph. International
775 Association of Scientific Hydrology. *Bulletin*, *15*(3), 25–33. https://doi.org/10.1080/02626667009493969
776 Wrede, S., Fenicia, F., Martínez-Carreras, N., Juilleret, J., Hissler, C., Krein, A., Savenije, H. H. G., Uhlenbrook,
777 S., Kavetski, D., Pfister, L. (2015). Towards more systematic perceptual model development: a case study
778 using 3 Luxembourgish catchments. *Hydrological Processes*, *29*(12), 2731-2750.
779 https://doi.org/10.1002/hyp.10393
780 Xu, Q., Liu, H., Ran, J., Li, W., & Sun, X. (2016). Field monitoring of groundwater responses to heavy rainfalls
781 and the early warning of the Kualiangzi landslide in Sichuan Basin, southwestern China. Landslides, 13,
782 1555-1570. https://doi.org/10.1007/s10346-016-0717-3
783 Yang, Y., Endreny, T. A., & Nowak, D. J. (2015). Simulating double-peak hydrographs from single storms over
784 mixed-use watersheds. *Journal of hydrologic engineering*, *20*(11), 06015003. https://doi.org/
785 10.1061/(ASCE)HE.1943-5584.0001225
786 Zhang, G. T., Cui, P., Gualtieri, C., Zhang, J. L., Ahmed Bazai, N., Zhang, Z. T., Wang, J., Tang, J. B., Chen,
787 R., Lei, M. Y. (2021). Stormflow generation in a humid forest watershed controlled by antecedent wetness
788 and rainfall amounts. *Journal of Hydrology*, 603. https://doi.org/10.1016/j.jhydrol.2021.127107
789 Zillgens, B., Merz, B., Kirnbauer, R., & Tilch, N. (2007). Analysis of the runoff response of an alpine catchment
790 at different scales. *Hydrology and Earth System Sciences*, *11*(4), 1441–1454. https://doi.org/10.5194/hess-
791 11-1441-2007
792

Appendix A: Supplementary Figures of Results and discussion

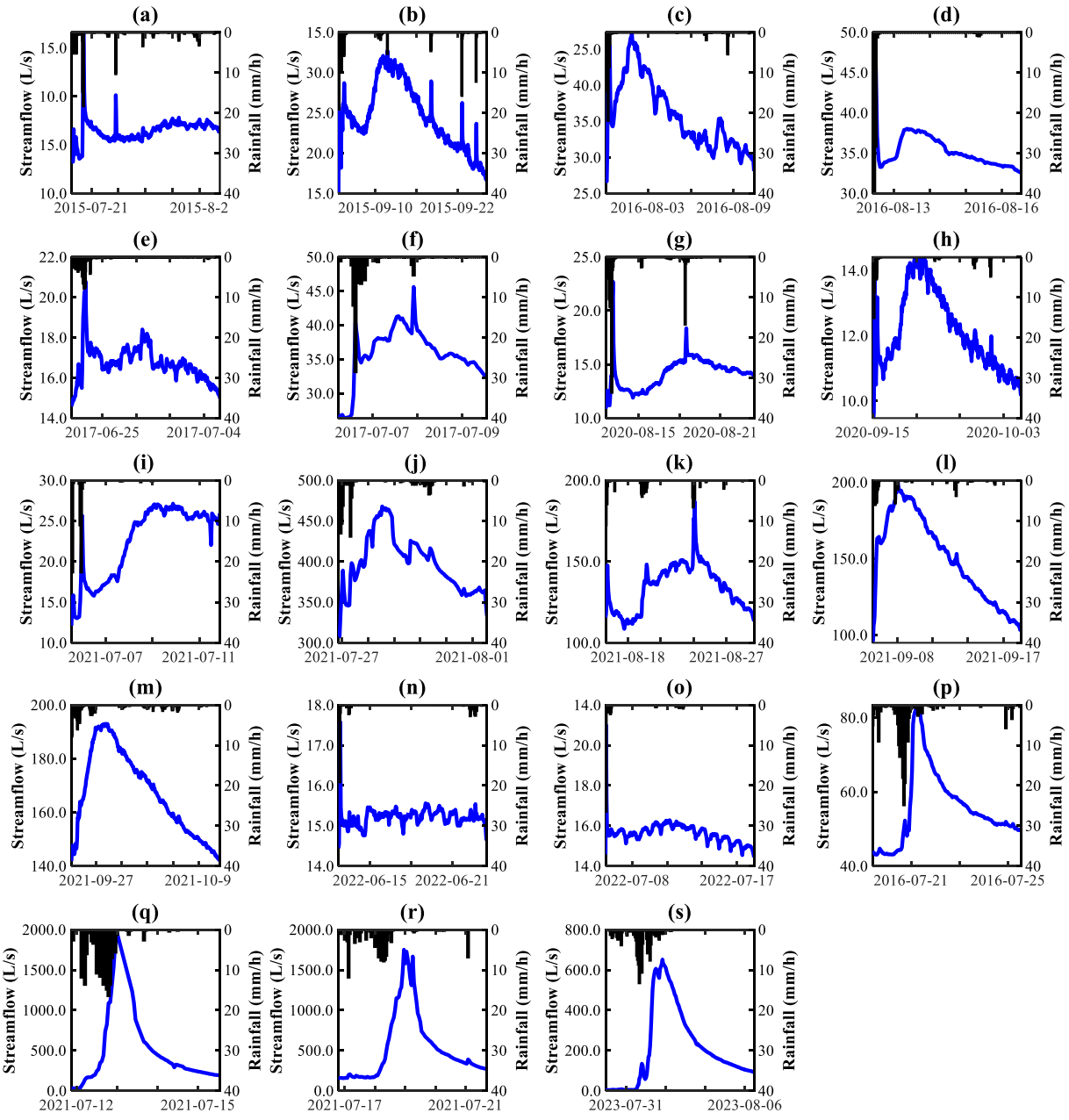

Figure A1. Rainfall and streamflow hydrograph for (a-o) 15 bimodal and (p-s) 4 hybrid bimodal events.